JCTC Journal of Chemical Theory and Computation

pubs.acs.org/JCTC Article

Nonadiabatic Excited-State Molecular Dynamics for Open-Shell Systems

Yu Zhang,* Linqiu Li, Sergei Tretiak, and Tammie Nelson*

Cite This: J. Chem. Theory Comput. 2020, 16, 2053−2064 Read Online

ACCESS | Metrics & More | Article Recommendations | Supporting Information

ABSTRACT: Nonadiabatic Molecular Dynamics (NAMD) of excited states has been widely used in the simulation of photoinduced phenomena. However, the inability to treat bond breaking and forming processes with single-reference electronic structure methods limits their application in photochemistry for extended molecular systems. In this work, the extension of excited-state NAMD for open-shell systems is developed and implemented in the NEXMD software. We present the spin-unrestricted CIS and TD-SCF formalism for the ground and excited states, analytical derivatives, and nonadiabatic derivative couplings for the respective potential energy surfaces. This methodology is employed to study the photochemical reaction of three model molecules. The results demonstrate the advantage of the open-shell approach in modeling photochemical reactions, especially involving bond breaking processes. We find that the open-shell method lowers the reaction barrier at the bond-breaking limits resulting in larger calculated photochemical quantum yields compared to the respective closed-shell results. We also address problems related to spin contamination in the open-shell method, especially when molecular geometries are far from equilibrium.

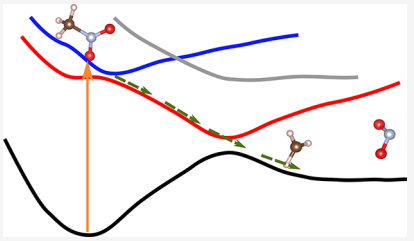

1. INTRODUCTION

Simulation of excited-state processes is indispensable to our understanding of photochemical and photophysical phenomena in molecular materials, such as photoisomerization, photodissociation, energy transfer, charge separation, and spatial localization of excitons.[1−8] Not only can such simulations aid in designing functional photoactive materials for a variety of technological applications, but also they provide unique theoretical insights into photophysical properties and mechanisms which are difficult to measure in experiments.[9−11] Modeling the photophysical and photochemical processes requires careful consideration of the time evolution of electronic populations spanning a manifold of electronic states with strong electron−nuclear coupling beyond the adiabatic Born−Oppenheimer regime.[12,13] The computational demands of such nonadiabatic simulations have led to the development of different methods. Because full quantum-mechanical treatments are expensive and limited to a few degrees of freedom,[14] the mixed quantum-classical nonadiabatic molecular dynamics (NAMD) has emerged as one of the most popular methods for the simulation of nonadiabatic phenomena.[15]

Over the years, our group has developed an excited-state NAMD framework to model photoinduced phenomena in molecular materials, such as organic conjugated materials (OCMs), that has been implemented in the Nonadiabatic EXcited state Molecular Dynamics (NEXMD) software package.[16−18] Briefly, Tully's fewest switches surface hopping (FSSH) method is used to calculate quantum transitions among excited states.[19] In FSSH, nuclei are treated classically, while electrons are treated quantum mechanically. The transition among excited states is determined stochastically based on the derivative nonadiabatic couplings (NACs). FSSH is a well-tested method for NAMD simulations that has become popular due to its balance between computational efficiency and accuracy across a variety of chemical systems.[13−15,18−23] In the NEXMD simulations, excited-state energies, their gradients, and NACs are computed, and trajectories are propagated on-the-fly.[24−29] At the single trajectory level, the NAMD simulations provide detailed insights into mechanistic and conformational information. On the other hand, properties such as excited-state lifetimes, nonradiative relaxation rates, and energy or change transfer rates are determined through averaging over an ensemble of trajectories. The statistical ensembles of trajectories can also be used to calculate photochemical quantum yields and branching ratios.

The calculation of both NACs and excited-state forces for nuclear propagation requires a proper description of excited states in the many-electron systems. In extended molecules, a large number of electrons and a dense manifold of excited states are involved. Therefore, an appropriate method must balance accuracy and computational cost. Methods like Hartree−Fock, while remarkably fast to compute, could not

Received: September 17, 2019
Published: March 2, 2020

https://dx.doi.org/10.1021/acs.jctc.9b00928
J. Chem. Theory Comput. 2020, 16, 2053−2064

give accurate excited-state electronic structure owing to a mono-orbital description of the excited state.[30−32] Time-dependent density functional theory (TD-DFT) and expensive multireference or multiconfigurational methods can provide accurate excited-state electronic structure but are computationally expensive when applied to large systems.[33,34] In NEXMD, the time-dependent self-consistent field (TD-SCF) formalism (such as configuration interaction singles, CIS) combined with a semiempirical model Hamiltonian (such as Austin Model 1, AM1[35]) is employed to achieve a reasonable accurate while computationally tractable description of excited states.[36,37] This method retains essential electronic correlations, and although it cannot describe states with significant double-excitation character, it is numerically efficient to compute and can treat excited-state dynamics in extended molecular materials.[38]

Our previous implementation of NEXMD is limited to the restricted closed-shell electronic structure representation. However, neither all molecules nor all states of closed-shell molecules can be described by pairs of electrons occupying closed-shell orbitals. This is especially true in photochemistry, where multiple spin states may be involved (i.e., radicals, fragments, etc.). In fact, open-shell pathways are known to be important even in systems with closed-shell reactants and products.[6] To exemplify the problem, consider the dissociation of H_2 which requires two electrons in a single orbital to split into two singly occupied orbitals at large distances (one on each hydrogen). In this case, a closed-shell description is inappropriate and results in H- with two electrons and H+ with no electrons. TD-DFT implementations of open-shell NAMD formalisms have been explored in previous studies.[6,39−41] However, the open-shell NAMD for extended molecular materials is still not available. Hence, we need to generalize the previous closed-shell TD-SCF formalism to accommodate open-shell situations where molecules have one or more unpaired electrons. When retaining a single-reference ground-state framework underpinning TD-SCF methods, there are two conventional approaches to deal with open-shell problems: the restricted open-shell and the unrestricted (U) open-shell procedure. In the restricted open-shell formalism, all electrons occupy closed-shell orbitals except for those electrons that are explicitly required to occupy open-shell levels. This procedure ensures that wave functions are eigenfunctions of the spin operator. However, the constraint of occupying orbitals in pairs raises the variational energy. The unrestricted open-shell procedure, on the other hand, can give a better description of energies by allowing all electrons to occupy open-shell orbitals. Since accurate descriptions of excited-state energies and reaction barriers are essential factors, formulation and efficient implementation of unrestricted methodology are essential in NAMD simulations.

In this work, we present an unrestricted TD-SCF framework for NAMD and its implementation in the NEXMD software. The developed methodology is then used to simulate the photochemistry of three molecular systems. Previous closed-shell excited-state NAMD simulations of these systems mainly focused on the first bond dissociation step.[1−3] An open-shell implementation can correctly account for unpaired electrons to describe fragment intermediates, which affects subsequent photochemical pathways and quantum yields. With the open-shell implementation, we can simulate the photochemical decomposition of photoactive materials through an excited-state process as excess electronic energy is transferred to vibrational modes.[1−3]

The manuscript is organized as follows. We first present the theory for the open-shell excited-state NAMD simulations in Section 2, including spin unrestricted CIS and TD-SCF frameworks for excited states in Section 2.1, spin contamination in Section 2.2, analytical gradients and nonadiabatic couplings in Section 2.3, and NAMD and FSSH algorithm in Section 2.4. Then we exemplify the methodology as implemented within the NEXMD package to perform simulations of photoinitiated bond breaking in prototype energetic materials. We compare our results to previous closed-shell reports of photochemistry for these systems in Section 3. Finally, this study is summarized in Section 4.

2. THEORETICAL METHODOLOGY

In this section, we describe details for the practical implementation of the spin-unrestricted open-shell method for nonadiabatic excited-state molecular dynamics.

2.1. Spin Unrestricted CIS and TD-SCF Frameworks for Excited States. Compared to the ground-state calculations, the calculations of electronic excited-state properties, including energies, gradients, and transition dipoles, are more complex due to the presence of many-body interactions. Various methods have been developed to treat these interactions at different levels of accuracy and efficiency. The TD-SCF framework is one of the more computationally efficient and popular methods.[26,39,42] TD-SCF is a general method for excited-state properties and can be implemented in the form of TD-DFT[26,39] or time-dependent Hartree−Fock (TDHF) or CIS methods.[42] In our work, we use the semiempirical formulation of the TD-SCF framework[42] as realized in the NEXMD software package.[18] TD-SCF solves the equation of motion (EOM) for the single electron density matrix of the molecule excited by an external field

$$\rho_{\mu\nu} = \langle \Psi(t)|c_\mu^\dagger c_\nu|\Psi(t)\rangle \tag{1}$$

where $\Psi(t)$ is the many-electron wave function, represented by a time-dependent single Slater determinant. $c_\mu^\dagger$ (c_ν) are creation (annihilation) operators in AO basis. In this manuscript, the following conventions are used: i, j, and k represent the occupied MOs, a and b represent unoccupied MOs, p and q label general orbitals, and μ, ν, κ, and λ represent the AO basis functions.

After excitation by an external field, the time-dependent density matrix can be represented in terms of a ground-state density matrix with perturbation, i.e., $\rho(t) = \rho_0 + \delta\rho(t)$, and the von-Neumann EOM for ρ is written as[42]

$$i\hbar\frac{\partial\rho}{\partial t} = [F(\rho), \rho] + [R(t), \rho] \tag{2}$$

where $F(\rho)$ is the Fock matrix, $R(t)$ is the external perturbation (usually induced by external field), and $\hbar$ is the reduced Planck constant. Within the linear response formalism, the EOM of eq 2 can be rewritten for the perturbation

$$i\hbar\frac{\partial\delta\rho}{\partial t} = \mathcal{L}(\delta\rho) + [R(t), \rho_0] \tag{3}$$

where the Liouville operator is defined as[43]

$$\mathcal{L}(x) \equiv [F(\rho_0), x] + [V(x), \rho_0] \tag{4}$$

The Fock matrix $F(x)$ is given by

https://dx.doi.org/10.1021/acs.jctc.9b00928
J. Chem. Theory Comput. 2020, 16, 2053−2064

$$F(x) = t + V(x) \tag{5}$$

where t is the one-electron integral accounting for the kinetic energy and nuclear attraction of an electron, and $V(x)$ is the Coulomb-exchange interaction. $\delta\rho(t)$ is readily solved by time-domain propagation of eq 3. Alternatively, eq 3 can be solved in the frequency-domain by solving the eigensolutions of $\mathcal{L}$. For the spin-unrestricted method implemented in this work, the density matrix, Fock, and Coulomb-exchange matrices are divided into two components, one component is for α spin and the other is for β spin. For instance, the Fock matrix is

$$F = \begin{bmatrix} F^{\alpha} & 0 \\ 0 & F^{\beta} \end{bmatrix} \tag{6}$$

where the off-diagonal block is set to zero because spin−orbit coupling is not considered in this work. The Coulomb-exchange matrix for spin σ is represented in the AO basis by

$$V^{\sigma}_{\mu\nu}(x) = \sum_{\kappa\lambda}\left[x_{\kappa\lambda}(\mu\nu|\kappa\lambda) - \frac{1}{2}(\mu\kappa|\nu\lambda)x^{\sigma}_{\kappa\lambda}\right] \tag{7}$$

where $x = x^{\alpha} + x^{\beta}$. μ, ν, κ, λ, and σ refer to spatial orbitals and spin space, respectively. $(\mu\nu|\kappa\lambda)$ are conventional two-electron integrals representing Coulombic interactions. Similar expressions for one- and two-electron components can be written for TD-DFT methodology.[26,44]

We can introduce a family of single-electron density matrices[45]

$$(\rho_{mn})_{\mu\nu} = \langle\psi_m|c^{\dagger}_{\mu}c_{\nu}|\psi_n\rangle \tag{8}$$

where indices m and n label the adiabatic electronic eigenstates of the system, and $\psi_{m/n}$ are the corresponding adiabatic wave functions. Thus, $\rho_{0m} = \zeta_m$ is the transition density matrix, which represents the changes in the density matrix induced by an optical transition from the ground state $|0\rangle$ to the excited state $|\psi_m\rangle$. These transition matrices are the eigenfunctions of the two-particle Liouville operator $\mathcal{L}$ from the linearized TDHF EOM[43]

$$\mathcal{L}\zeta_m = \Omega_m\zeta_m \tag{9}$$

The eigenvalue Ω_m represents the electronic transition energy of the $|0\rangle \rightarrow |\psi_m\rangle$ excitation. The eigenvectors are subject to the normalization conditions.[43]

In general, the MO representation provides a more clear physical picture of the excitation and enables the decomposition of all possible transitions among occupied and unoccupied virtual orbitals. Thus, eq 9 in MO representation can be rewritten as[39,42,46]

$$\begin{bmatrix} A & B \\ -B & -A \end{bmatrix}\begin{pmatrix} X \\ Y \end{pmatrix} = \Omega\begin{pmatrix} X \\ Y \end{pmatrix} \tag{10}$$

which is known as the first-order RPA equation.[46] A and B are submatrices defined in the Liouville space $[(N_vN_o) \times (N_oN_v)]$ where N_o and N_v are the number of occupied and unoccupied (virtual) molecular orbitals, respectively. A and B matrix elements in the MO basis are

$$\begin{aligned} A_{ia\sigma,jb\sigma'} &= (\epsilon_a - \epsilon_i)\delta_{ij}\delta_{ab}\delta_{\sigma\sigma'} + (ia\sigma|jb\sigma') - (ab|ij)\delta_{\sigma\sigma'} \\ B_{ia\sigma,jb\sigma'} &= (ia\sigma|jb\sigma') - (ja|ib)\delta_{\sigma\sigma'} \end{aligned} \tag{11}$$

where i, $j(a, b)$ run over occupied (unoccupied) molecular orbitals, and ϵ_a and ϵ_i denote energies of molecular orbitals.

In eq 11, matrices A and B are Hermitian. Matrix A is identical to the CIS matrix.[47] Thus, diagonalization of A gives the CIS excitation energies by neglecting the B matrix and Y vector, whereas the Hermitian matrix B represents higher order electronic correlations.[43] An approximate solution to the full matrix equation can be found by neglecting B and Y which is known as the CIS formalism or Tamm-Dancoff approximation for DFT.[48,49] For a majority of molecules, the X component dominates because elements of B are small compared to those of matrix A. The first term of A, as shown in eq 11, is the zeroth-order approximation to the excitation energies which is simply the energy difference between the single-particle energies (eigenvalues of the Fock matrix). The rest of the terms in A and B matrices are the additional Coulomb and exchange-correlation screening of the excitation process.

The X and Y components of the eigenvector (transition density matrix) in the MO representation, i.e., $\xi = \binom{X}{Y}$, are the particle-hole (ph) and hole-particle (hp) components, respectively. For the unrestricted formalism, the transition density matrix contains α and β spin parts, i.e.,

$$\xi = \begin{pmatrix} \xi^{\alpha} \\ \xi^{\beta} \end{pmatrix}, \quad \text{where} \quad \xi^{\sigma} = \begin{pmatrix} X^{\sigma} \\ Y^{\sigma} \end{pmatrix} \tag{12}$$

in the MO space. In closed-shell calculations, $\xi^{\alpha} = \xi^{\beta}$ for singlets and $\xi^{\alpha} = -\xi^{\beta}$ for triplets, respectively. Thus, the spin degree of freedom can be dropped in the closed-shell methods. However, in spin-unrestricted methods, there is no such relation between the ξ^{α} and ξ^{β}. Thus, the spin degree of freedom should be included explicitly as described in eq 11. In this work, spin-unrestricted TD-SCF including UCIS are implemented.

2.2. Spin Contamination. One of the fundamental problems for unrestricted quantum-chemical simulations is so-called spin contamination being an artificial mixing of different electronic spin states. Here we outline numerical approaches tracking this issue in excited-state NAMD for the TD-SCF (or UCIS) method. Ground-state UHF wave functions can suffer from spin contamination. Since the UCIS wave function consists of substitutions from the ground-state UHF reference, it is reasonable to expect that molecules with a spin-contaminated ground state will have the same, or even larger, spin contamination in the UCIS excited states. Thus, the expectation value of the total spin-squared operator, $\langle\hat{S}^2\rangle$, should be calculated to monitor the spin contamination. Evaluation of $\langle\hat{S}^2\rangle$ of the m^{th} excited state is straightforward[47]

$$\langle\hat{S}^2_m\rangle = S^2_U - \sum_{\sigma,ab} Q^{\sigma}_{ab}P^{\sigma}_{ab} - \sum_{\sigma,ij} Q^{\sigma}_{ij}P^{\sigma}_{ij} - 2\sum_{ijab}\Delta_{ij}\Delta_{ab}c^{\alpha}_{ia}c^{\beta}_{jb} \tag{13}$$

where Δ_{pq} is the α−β MO overlap, the definitions of Q and P can be found in ref 47, and S^2_U is the $\langle\hat{S}^2\rangle$ of the UHF reference

$$S^2_U = \Delta N(\Delta N + 1) + N_{\beta} - \sum_{ij}|\Delta_{ij}|^2 \tag{14}$$

where $\Delta N = \frac{N_{\alpha} - N_{\beta}}{2}$ with N_{σ} being the number of spin σ electrons.[47]

https://dx.doi.org/10.1021/acs.jctc.9b00928
J. Chem. Theory Comput. 2020, 16, 2053−2064

Eq 13 indicates that the origin of a spin contaminated excited state is 2-fold. Spin contamination in the excited state can arise through differences in the spatial parts of the α and β orbitals, as in the ground state, as well as the differences in the α and β excitation coefficients. Consequently, for a relatively spin pure ground state, it is still possible to get impure excited states using the spin-unrestricted method. For pure excited states, we can roughly get $\xi^{\alpha} \simeq \pm \xi^{\beta}$, and thus the transition dipole vanishes for the triplet-like states. It is important to note that in the NAMD simulations, the signs of transition density matrices of each spin component $\xi^{\alpha/\beta}$ are checked at every time step to avoid a sudden change in the phase of the transition density matrix of each spin.

2.3. Analytical Gradients and Nonadiabatic Couplings. For propagating molecular dynamics along the potential energy surface (PES), the gradients (forces) on the PES, i.e., $\nabla_{\mathbf{R}} E_m(\mathbf{R})$, should be calculated efficiently to achieve a longer time scale of simulations. Thus, an analytical gradient technique, which is much faster than the respective numerical differentiation, should be developed. The analytical gradient for the ground-state energy calculated from the SCF procedure is trivial according to the variational principle[50]

$$\nabla_{\mathbf{R}} E_0(\mathbf{R}) = \frac{1}{2}\sum_{\sigma} \mathrm{Tr}[(\nabla_{\mathbf{R}} t + \nabla_{\mathbf{R}} F^{\sigma})\rho_0^{\sigma}] \tag{15}$$

Here the trace goes over the spatial variable. The derivatives in the above equation only apply to the one-electron and two-electron operators according to the Hellmann−Feynman principle.[51]

The calculation of gradients of the excited-state energies ($E_m = E_0 + \Omega_m$) is more complicated. Following the detailed derivation in refs 25, 26, and 44, the gradient of the transition energy is written in terms of the excited-state density matrix

$$\nabla_{\mathbf{R}} \Omega_m = \sum_{\sigma} \mathrm{Tr}[(\nabla_{\mathbf{R}} F^{\sigma}) P_m^{\sigma}] + \mathrm{Tr}[(\nabla_{\mathbf{R}} V^{\sigma}(\xi_m))\xi_m^{\sigma}] \tag{16}$$

where $P_m^{\sigma} = \rho_{mm}^{\sigma} - \rho_{00}^{\sigma}$ is related to the difference between excited- and ground-state density matrices, and it is composed of two terms

$$P_m^{\sigma} = 2T_m^{\sigma} + Z_m^{\sigma} \tag{17}$$

where $T_m^{\sigma} = \frac{1}{2}[[(\xi_m^{\sigma})^{\dagger}, \rho_{00}^{\sigma}], \xi_m^{\sigma}]$ is the unrelaxed part of the excited-state density matrix. Z_m^{σ} represents the orbital relaxation effects and can be solved through a linear equation

$$\mathcal{L} Z_m^{\sigma} = -[([[\rho_{00}^{\sigma}, (\xi_m^{\sigma})^{\dagger}], V^{\sigma}(\xi_m)] + V^{\sigma}(T_m)), \rho_{00}^{\sigma}] \tag{18}$$

The iterative biconjugate gradient stable (BICGStab)[52] method is employed to solve the above equation. To demonstrate the validity of eq 16, we calculated the relative error of the analytical gradients compared to the numerical gradients for 500 different configurations of nitromethane on two different states. The comparison, shown in Figure S1, demonstrates that relative error is generally less than 0.01%.

For molecular dynamics with quantum transitions, the NAC vector (NACR) is also needed from the electronic structure calculations. The NACR between two states is defined as

$$\mathbf{d}_{mn} = \langle \psi_m(\mathbf{R}) | \nabla_{\mathbf{R}} \psi_n(\mathbf{R}) \rangle, \; m \neq n \tag{19}$$

The NACR can also be calculated analytically by making use of the Hellmann−Feynman theorem[53,54]

$$\mathbf{d}_{mn} = \frac{\sum_{\sigma} \mathrm{Tr}[\nabla_{\mathbf{R}} F^{\sigma} \rho_{mn}^{\sigma}]}{\Omega_m - \Omega_n}, \; m \neq n \tag{20}$$

where $\rho_{mn}^{\sigma} = [[\xi_m^{\sigma}, \rho_{00}], \xi_n^{\sigma}]$. Similarly, the time-dependent NAC scalar (NACT) is given by

$$\dot{\mathbf{R}} \cdot \mathbf{d}_{mn} = \frac{\sum_{\sigma} \mathrm{Tr}[\nabla_t F^{\sigma} \rho_{mn}^{\sigma}]}{\Omega_m - \Omega_n}, \; m \neq n \tag{21}$$

As argued in Section 2.2, we can get $\xi^{\alpha} \simeq \pm \xi^{\beta}$ for pure excited states. Hence, if m and n are corresponding to singlet-like and triplet-like states, respectively, the density matrices between the two adiabatic states satisfy $\rho_{mn}^{\alpha} = -\rho_{mn}^{\beta}$. Consequently, the NACs (NACR and NACT) vanish automatically between the singlet- and triplet-like states, i.e., there are no transitions between different spin states.

2.4. NAMD and FSSH Algorithms. Excited-state energies, gradients, and NACs are the essential ingredients for NAMD simulations. Thus, the open-shell formalism presented in Sections 2.1−2.3 is applicable to any NAMD algorithm, such as Ehrenfest, FSSH, and multiconfigurational Ehrenfest with multiple cloning approaches.[55−57] In this work, the open-shell formalism is implemented using the FSSH algorithm as a representative application. Within FSSH, the time-dependent Schrödinger equation (TDSE) for both electrons can be solved via the EOM of $c_m(t)$ (the expansion coefficient of the total time-dependent electronic wave function for adiabatic state m) as

$$i\hbar \dot{c}_m(t) = c_m(t) E_m(t) - i\hbar \sum_n c_n(t) \dot{\mathbf{R}} \cdot \mathbf{d}_{mn} \tag{22}$$

where $E_m(\mathbf{R})$ is the energy of adiabatic state m. The $\dot{\mathbf{R}} \cdot \mathbf{d}_{mn}$ represents the NACT between two states. Tully's FSSH formalism is employed to model the electronic transitions between PESs.[19] The hops between adiabatic states are accepted or rejected stochastically by comparing the generated random number and calculated switching probability g_{mn}[18]

$$g_{mn} = \frac{\sum_k^{N_q} b_{nm}(k)\delta t}{\alpha_{mn}} \tag{23}$$

where $N_q = \Delta t/\delta t$ with Δt (δt) being the classical (quantum) time step, $b_{nm} = -2\mathrm{Re}(a_{mn}^{*} \dot{\mathbf{R}} \cdot \mathbf{d}_{mn})$, and $a_{mn} = c_m c_n^{*}$ is the time-dependent element of the density matrix. Following the hop, energy is conserved through rescaling nuclear velocities along the direction of NACR. Electronic decoherence[58] and transitions at unavoided (trivial) crossings[59] were also treated within the NEXMD framework.

On the excited-state PES, nuclei evolve according to constant temperature Langevin dynamics or energy-conserving Newtonian dynamics

$$M_a \ddot{\mathbf{R}}_a(t) = -\nabla_a E_m(\mathbf{R}) - \gamma M_a \dot{\mathbf{R}}_a(t) + \eta(t) \tag{24}$$

Here M_a, $\ddot{\mathbf{R}}_a(t)$, and $\dot{\mathbf{R}}_a(t)$ are the mass, acceleration, and velocity of the a^{th} nucleus. $\eta(t)$ is the random force determined by the damping coefficient γ and bath temperature T (or thermostat). The Langevin equation reduces to energy-conserving Newtonian motion when $\eta(t)$ and γ are set to zero.

Since we use FSSH to model electronic transitions, the result is a statistical average over an ensemble of trajectories. For each trajectory, initialization of adiabatic state coefficients is determined through a Gaussian shaped Franck−Condon window

https://dx.doi.org/10.1021/acs.jctc.9b00928
J. Chem. Theory Comput. 2020, 16, 2053−2064

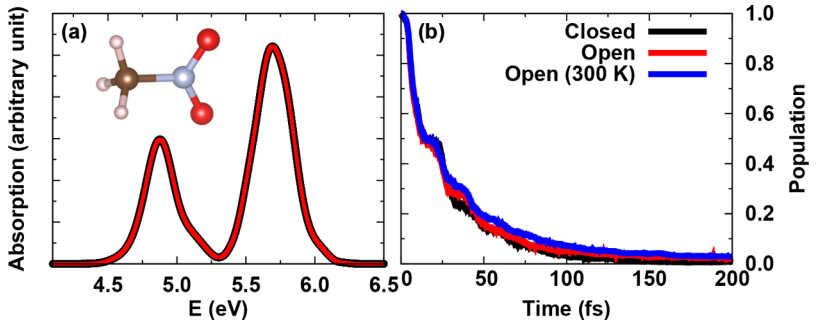

Figure 1. (a) The absorption spectrum of NM using closed- (black dots) and open-shell (red line) implementations. The triplet-like states calculated from the open-shell method are dark states which do not contribute to the absorption spectrum. (b) Time evolution of adiabatic state ($n\pi^*$) population average. The initial $n\pi^*$ state shows an exponential decay. Fitting the population dynamics to an exponential decay shows that the lifetimes of the $n\pi^*$ state are 26.0 and 26.8 fs for closed- and open-shell methods, respectively. The relaxation is slowed down (29.9 fs) if the NM molecule is coupled to a bath of 300 K.

$$f_m = \frac{1}{\Gamma\sqrt{2\pi}} \exp\left[-\frac{(\omega - \Omega_m)^2}{2\Gamma^2}\right] \tag{25}$$

where ω denotes the excitation energy, Ω_m is the energy of state m, and Γ is related to the full width at half-maximum as $FWHM = 2\Gamma\sqrt{2\ln 2}$. Oscillator strengths for each state are weighted by f_m. The initial state is chosen by comparing the normalized weighted values with a random number.

3. RESULTS AND DISCUSSION

3.1. Simulation Details. To test our open-shell NEXMD formalism, we have run NEXMD simulations of three model systems, nitromethane (NM), tetrazole [1,5-*b*] [1,2,4,5] tetrazine-6-amine with one oxygen substitution (ATTO), and tetrazine dichloride substituted derivative of pentaerythritol tetranitrate (PetrinTzCl). All ground-state geometries were initially optimized with the semiempirical AM1[35] technique in NEXMD.[18] For each system, constant-temperature ground-state adiabatic molecular dynamics using a 0.5 fs time step was performed for 300 ps through Langevin dynamics to equilibrate to 300 K. 500 snapshots were evenly taken from the equilibrated ground-state trajectories. For each snapshot, the unrestricted TD-SCF method was used to calculate oscillator strengths and vertical excitation energies of relevant excited states, which were then used to compute the linear absorption spectra. The initial excitations were determined through a Gaussian-based Franck−Condon window with an empirical standard deviation of 0.5 eV. The NAMD simulations were started from each snapshot and propagated independently using energy-conserving Newtonian dynamics.

We do not use constant-temperature Langevin dynamics for NAMD because of ultrafast time scales involved in the decomposition pathways. Decomposition involves bond breaking, which requires a certain amount of excited vibrational energies. Typically, Langevin dynamics damps the energy and leads to reduced yields being another extreme. To confirm this point, we also demonstrate the effect of Langevin dynamics on photochemical reactions in the example of the NM molecule. Finally, we averaged over all trajectories to obtain excited-state lifetimes, and photochemical quantum yield was determined as the fraction of trajectories that undergo bond breaking reaction.

The NEXMD simulations of isolated molecules were then started from the different photoexcited configurations. We used the same parameters to run NEXMD with closed- and open-shell methods for NM, ATTO, and PetrinTzCl. For NM, the initial excitation is chosen to be the $\pi^* \leftarrow n$ transition. Newtonian dynamics is employed to propagate each independent trajectory with a classical time step of Δt = 0.1 fs and a quantum time step of δt = 0.025 fs. The quantum time step is reduced by a factor of 10 to locate the trivial unavoided crossings, and the instantaneous decoherence correction was employed to introduce electronic decoherence. 500 different initial geometries and momenta taken from the ground-state dynamics were chosen to propagate NAMD. In both open- and closed-shell simulations, the nonadiabatic transitions to S_0 are not explicitly simulated due to the inability to describe crossings between a multireference UCIS/CIS excited state and a single reference UHF/HF ground state.[60] Alternatively, we introduce a simple model to treat the transition to the ground state: when the system is in the lowest energy excited state and the ground-state spin contamination is larger than a certain limit (0.5 in this work), transition to the ground state is enforced. (It will be clear later from the PES of nitromethane that the spin contamination emerges after the Coulson-Fischer (CF) point, in which regime the energy gap between the excited states and ground states becomes smaller.) In addition, we can also trigger hopping to the ground state if the system is in the lowest energy excited state and the energy gap between the excited state and ground state is smaller than a certain value. Similar models were previously utilized for describing nonadiabatic dynamics when transitioning to the ground state in the framework of the single-reference TD-DFT method.[6] When the criterion of hopping to the ground state is satisfied, the MD is changed to adiabatic propagation on the ground-state PES, and all the velocities are rescaled to ensure energy conservation. This simple model is termed as "Open-GS" and is used to compare to the results without hopping to the ground state.

3.2. Nitromethane. Being the simplest nitroalkane, NM's photodecomposition has been the subject of numerous experimental and theoretical investigations.[1,61−64] Because of the large amount of data related to NM's photodecomposition process, NM becomes a good benchmark system to test the validity of new methods. Here we compare NM photochemical properties using closed- and open-shell NAMD implementations. Figure 1(a) shows the results of the computed linear absorption spectrum for gas-phase NM. To calculate the absorption spectra, single-point calculations at sampled ground-state geometries were performed to determine excited-state energies and oscillator strengths. Oscillator

https://dx.doi.org/10.1021/acs.jctc.9b00928
J. Chem. Theory Comput. 2020, 16, 2053−2064

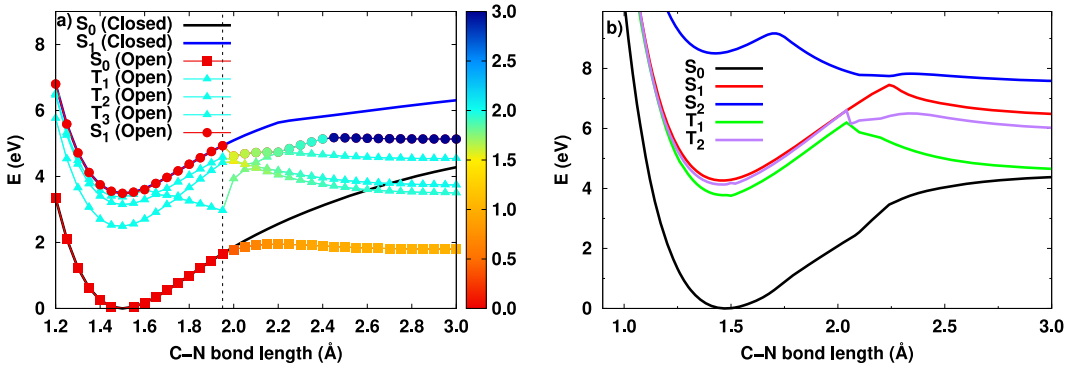

Figure 2. a) PESs of NM along the reaction path of C−N breaking. Dotted and solid lines are calculated from the open- and closed-shell methods, respectively. The S_1 and T_1−T_3 states are singlet-like and triplet-like states when the molecule is close to its equilibrium configuration, respectively. The color of the dotted lines shows the $\langle S^2 \rangle$ of the states. The change in color demonstrates the evolution of spin contamination of each state along the reaction coordinate. The plots indicate the reaction barriers calculated by open-shell are significantly reduced. The black dashed line marks the kink at the CF point. b) PESs calculated at the level of XMS-CASPT2.

strengths were broadened with a Gaussian-shaped Franck−Condon window centered at the excitation energies with an empirical standard deviation of 0.10 eV. The total absorption spectrum was then calculated as an average over all the spectra of sampled ground-state conformations. Both the open-shell and closed-shell methods give the same absorption spectrum. NM is known to have two absorption peaks in the UV region, which are assigned to the $\pi\pi^*$ transition with experimental maximum around 200 nm (6.2 eV) and the $n\pi^*$ transition with experimental maximum around 270 nm (4.6 eV).[65] Compared to the experiment, the calculated absorption spectrum shows a blue-shifted $n\pi^*$ transition. To produce the spectrum shown in Figure 1, the open-shell method requires the calculation of 20 excited states (roughly 10−12 of them are triplet-like states), whereas the closed-shell method only requires 10 singlet states. Because $\xi^{\alpha} \simeq -\xi^{\beta}$ for these triplet-like states, the transition dipole is several orders of magnitude smaller than that of the singlet-like states. Consequently, the triplet-like states calculated from the open-shell method are dark states and have no contribution to the absorption spectrum.

The time evolutions of $S_{n\pi^*}$ populations with closed- and open-shell implementations are shown in Figure 1(b). The $S_{n\pi^*}$ population is fit through a single exponential decay function with the form $f(x) = \exp(-x/\tau)$ where τ represents the lifetime. The lifetimes obtained from the closed- and open-shell methods are 27.5 and 27.4 fs, respectively. The two lifetimes are almost the same. It is trivial that the two methods give similar lifetimes. Initial electronic structures calculated from the two methods are identical except that many additional triplet-like states are obtained from the open-shell method, and the nonadiabatic transition only occurs between the singlet-like states for the open-shell method. This is an example of a photophysical process where the bond breaking and higher spin states are not involved. Experiments report the $n\pi^*$ state lifetime to be 36 fs.[66] Both closed- and open-shell methods predicted smaller lifetimes than expected. This may result from isolating molecules from the environment, i.e., bath, when running NEXMD simulations. When the molecule is isolated, electronic energy can only dissipate to vibrations and not into the environment. Hence, the nuclear velocities are larger than that with dissipation into environment, which results in faster relaxation dynamics. If the energy exchange between NM and the environment (by introducing thermostat) is introduced, the excited-state lifetime becomes longer. To illustrate the effect of the bath on chemical reactions, we performed additional constant temperature NAMD simulations using Langevin dynamics for NM with T and γ being 300 K and 10 ps^{-1}, respectively. As shown by the blue line of Figure 1(b), when the molecule is coupled to a bath, the relaxation $S_{n\pi^*}$ is slightly slower (30 fs). In general, the relaxation is reduced with increasing friction coefficient γ.[17]

According to a previous theoretical study, it was shown that there are three possible reaction pathways for nitromethane following photoexcitation to the $n\pi^*$ state:[1] 1) C−N bond breaking; 2) C−N−O to C−O−N (nitro-nitrite) isomerization; and 3) proton transfer (aci-nitromethane formation). The dominant dissociation pathway is C−N bond breaking resulting in dissociation of NO_2.[1] The open-shell simulations also recover the three expected reaction pathways, and C−N bond breaking is still the dominant pathway. However, the nitro-nitrite isomerization becomes a rare event in open-shell simulations. This phenomena can be easily understood from the potential energy surfaces (PESs) of NM. Figure 2(a) shows PESs along the C−N reaction coordinate. We observe that the open-shell ground-state energy decreases with increasing C−N bond distance after the C−N bond distance is larger than 2.2 Å. Hence, the open-shell simulations result in larger C−N separation. Since the nitro-nitrite isomerization is following the C−N bond breaking, this process is less likely when C−N separation is larger. Therefore, we focus on C−N breaking in the comparison of closed- and open-shell simulations. From Figure 2(a), the reaction barrier of open-shell PESs is significantly reduced compared to the closed-shell PESs because the unrestricted method gives smaller ground and excited energies at the bond-breaking limit. For the closed-shell method, the electrons are always shared no matter how far atoms are separated because spin components in each electron pair share the same spatial orbitals. In contrast, the unrestricted open-shell method does not restrict different spins in an electron pair to the same spatial orbital and thus can treat electrons properly at dissociation. In particular, for open-shell PESs (Figure 2(a)) we see a kink indicating a crossing between ground state and one of the mixed spin states at the C−N distance of about 2 Å, which provides a dissociative path back to the ground state, which is missing for closed-shell simulations. It should be noted that the kink marked by the black dashed line in Figure 2(a) represents the CF point.[67−69] Before the CF point, there is no spin contamination. The

https://dx.doi.org/10.1021/acs.jctc.9b00928
J. Chem. Theory Comput. 2020, 16, 2053−2064

calculated states have pure singlet or triplet character. Beyond the CF point, spin contamination becomes significant, and a sharp kink in the PES may emerge. These unphysical sharp kinks may be attributed to the lack of double excitation, according to a recent study.[69] For comparison, we also performed high-level *ab initio* XMS-CASPT2 calculations by employing the BAGEL package[70−72] as shown in Figure 2(b). The computational details can be found in the SI. The comparison indicates that the semiempirical PESs obtained from the unrestricted open-shell method agree qualitatively with the *ab initio* XMS-CAPST2 data except the unrestricted open-shell T_1 state has a dip at the CF point (Figure 2(a)).

Figure 3 plots the histogram of the maximum C−N distance from each NEXMD trajectory calculated from the closed-shell

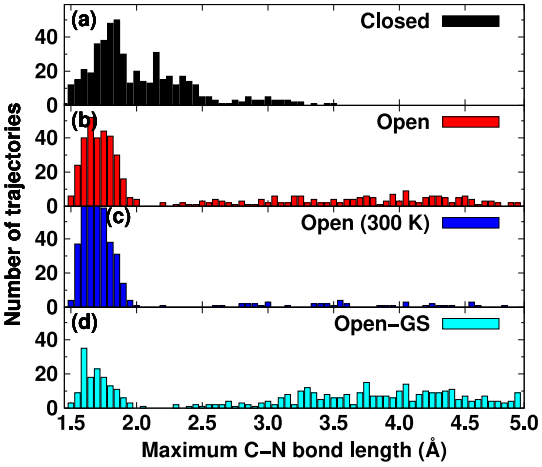

Figure 3. Histogram of the maximum C−N bond length from each NEXMD trajectory calculated from (a) closed-shell, (b) open-shell, (c) open-shell with thermostat, and (d) Open-GS methods, respectively.

(a), open-shell (b), open-shell with thermostat (c), and Open-GS (d). The results show that the majority of C−N distances reside within 1.5−2.2 Å for both open- and closed-shell methods. Compared to the closed-shell results, the open-shell calculations reach longer C−N distances. The probability of longer C−N distances is further increased if the transition to the ground state is allowed. In contrast, if the thermostat is introduced, the energy dissipation into the bath significantly reduces the probability of longer C−N distances, an indication that the molecule loses energy through dissipation before it can overcome the reaction barrier and trigger the chemical reaction. If smaller friction is used in the Langevin dynamics, the energy dissipation is reduced, and the probability of longer C−N distances can be increased. Because the open-shell ground-state PES shows a turning point at 2.2 Å, as shown in Figure 2(a), we define C−N bond breaking if the maximum C−N distance is larger than 2.2 Å. This threshold was also employed in previous work.[1] The analysis of 500 trajectories found that C−N breaking occurs in 169 and 216 trajectories giving the predicted quantum yields (QYs) of 33.8% and 43.6% for closed- and open-shell methods, respectively. In NEXMD, the photochemical QY is defined as the fraction of trajectories that exhibit a particular bond breaking event. The open-shell method gives larger QY compared to the closed-shell method consistent with the reduced open-shell reaction barrier as shown in Figure 2(a) discussed above. If Langevin dynamics is used, the QY is reduced to 9.0% (45 trajectories) as a result of energy dissipation into the bath. In contrast, QY is increased to 71.8% (359 trajectories) for the Open-GS method. Because the crossing points between T_{1-3} and ground state are located near the peak in the ground-state reaction barrier as shown in Figure 2(a), the additional kinetic energy gained from hopping to the ground state generally suffices to overcome the reaction barrier and leads to *C*−*N* bond breaking. Consequently, the QY is significantly enhanced.

Since the unrestricted TD-SCF/CIS methods are used, there is unavoidable spin contamination beyond the CF point. Consequently, there may be transitions between the impure states beyond the CF point due to the spin contamination. Our numerical simulations reveal that the dynamics can evolve on the T_{1-3} states after entering the regime beyond the CF point, which also confirms there are transitions between the impure states. However, the lower barrier on the PESs is not the result of spin contamination. Recent work by Head-Gordon's group demonstrated that the unrestricted open-shell ground-state PES of H_2 is close to the exact solution even though there is spin contamination beyond the CF point.[69] Because the barrier of the ground-state PES is significantly lowered by the open-shell method, the reaction barriers of the excited state are also reduced accordingly. Subsequently, open-shell calculations are more appropriate for describing bond breaking compared to their closed-shell counterparts. In addition, the barriers (as well as PES landscapes) calculated by the unrestricted open-shell method agree qualitatively with the high-level XMS-CASPT2 results as shown in Figure 2. The benchmark calculation against XMS-CASPT2 shown in Figure 2 found that the excited-state PESs turn over near the CF point. These lowest excited-state PESs show dissociative feature beyond the CF point. Therefore, the probability of overcoming the barrier and reaching the dissociation regime is not affected by the spin contamination. Even though these initially pure states become mixed beyond the CF point, the dynamics already reaches the dissociation regime, and the dissociation is readily triggered regardless of whether there are unphysical transitions between these mixed states or not. Hence, the unphysical transitions beyond the CF point have a limited effect on the QY of chemical reactions. Especially, the Open-GS method will switch the dynamics to the ground-state PES once the system is on the lowest excited state and goes beyond the CF point such that the effect of the unphysical transitions can be further suppressed, but this issue may vary for different systems. During the dynamics, the $\langle \hat{S}^2 \rangle$ is calculated at each step to monitor the spin contamination. Special attention should be paid to check whether the spin contamination introduces unphysical results for each particular case.

3.3. ATTO. We next examine the NAMD of ATTO, an optically active OCM predicted to have large one- and two-photon absorption cross sections[73] making it a desirable candidate for optically initiated photodecomposition mechanism. The optical properties and photochemistry of ATTO have been the subject of previous theoretical investigations which used closed-shell NAMD simulations.[2,73] As expected, the calculated absorption spectra calculated using closed- and open-shell methods are the same, as shown in Figure 4(b). However, the open-shell required the calculation of 35 excited states in the 5.0 eV energy range, whereas the closed-shell required only 13 states. The calculated absorption spectra exhibit a red-shift compared to the experimentally measured spectrum.[2] Consistent with previous studies, we choose the excitation wavelength to be 3.5 eV (355 nm)[2] for both closed-

https://dx.doi.org/10.1021/acs.jctc.9b00928
J. Chem. Theory Comput. 2020, 16, 2053−2064

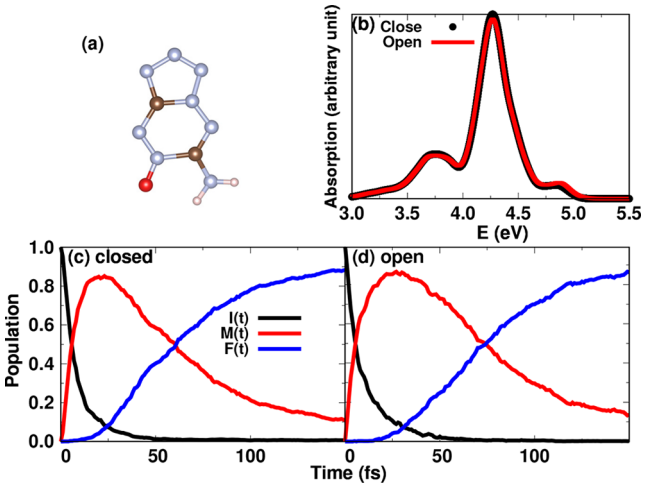

Figure 4. a) Geometry of the ATTO molecule. b) Absorption spectrum of ATTO using closed-shell (black dots) and open-shell (red line) implementations. Time evolution of adiabatic-state populations during (c) open- and (d) closed-shell NEXMD simulations of ATTO used for the three-state kinetic model, where $I(t)$, $M(t)$, and $F(t)$ represent the initial, intermediate, and the final states, respectively. The corresponding time scales are shown in Table 1.

and open-shell corresponding to the wavelength of the Nd:YAG laser typically employed in spectroscopic experiments. This 355 nm, though not consistent with absorption maxima, is aligned with the onset of the absorption peak.

A three-state sequential irreversible kinetic model $I(t) - M(t) - F(t)$ is used to depict excited-state dynamics in ATTO, in which $I(t)$ is the averaged population of all initially excited states, $M(t)$ represents the averaged sum of the intermediate-state populations, and $F(t)$ is the averaged population of the final state. For the closed-shell, the final state is the first excited-state S_1. While, for the open-shell method, the dynamics may relax to the lowest few states since these states are close and some of them are triplet-like states or mixed excitation states. Similar to nitromethane (Figure 2), ATTO also has few open-shell excited states lower than the closed-shell S_1 state. Therefore, the S_1−S_3 states are defined as the final states for the open-shell method. In addition, a range of states from S_3 to S_8 (S_{12} to S_{17} for open-shell) in ATTO corresponds to the initial state because of the conformational disorder in the thermal ensemble. Rate constants k_1 and k_2 are obtained through fitting the following equations

$$I(t) = e^{-k_1 t}$$

$$M(t) = \frac{k_1}{k_2 - k_1}(e^{-k_1 t} - e^{-k_2 t})$$

$$F(t) = 1 - M(t) - I(t) \quad (26)$$

The resulting initial state lifetime ($\tau_1 = k_1^{-1}$) and relaxation time ($\tau_M = k_2^{-1} + k_3^{-1}$) are shown in Table 1, together with the total photochemical QYs. Here we do not focus on any particular bond breaking pathway and instead report the total photochemical QY. k_1 represents the lifetime of the initial excited state, and $k_1 + k_2$ represents the total relaxation time scale.

The evolution of the relevant state populations and PES are shown in Figure 4(c,d). Our closed-shell result gives an initial excited state lifetime of 8.1 fs and a total relaxation time scale of 71.1 fs, which is close to the previously published results.[2] The open-shell results give a similar lifetime for the initial excited state of 8.7 fs (8.5 fs for the Open-GS method). This is reasonable because the initial electronic structures around the equilibrium positions are identical and consist only of pure states, which is also consistent with the population dynamics of NM shown in Section 3.2. However, the open-shell method cannot give pure singlets or triplets when the molecule is far from equilibrium positions where the initial (singlet-) triplet-like states become mixed excitations. Consequently, the open-shell dynamics may end up with an additional transition pathway from the initial states to the final mixed states. Moreover, there are more states involved in the open-shell dynamics, and the final states of open-shell are different from those of closed-shell. As a result, the total relaxation time obtained from the open-shell method (92.1 fs) is significantly longer than that of closed-shell. We did not calculate the relaxation time for the Open-GS method since the final state, in this case, is ground state making the comparison meaningless.

Table 1. Results of the Excited-State Lifetimes and Relaxation Time Scales from the Three-State Sequential Kinetic Model

method	excited-state lifetime τ_I (fs)	relaxation time τ_M (fs)	QY (%)
closed-shell	8.1	71.1	90.2
open-shell	8.7	92.1	93.0
Open-GS	8.5		80.0

The photodissociation of ATTO can occur through several different pathways.[2] After considering all possible bond-breaking pathways, the closed-shell method results in a QY of 90.2%, which is slightly lower than the open-shell result of 93.0%, as expected. Because open-shell predicts a lower PES at the bond breaking length, the energy barrier for bond breaking should be smaller, resulting in larger QY as described in Section 3.2. However, for the Open-GS method, the QY is reduced to 80.0%. The situation is different from the case of NM where the QY is increased for the Open-GS method. After carefully checking the dynamics of several trajectories, we found that some trajectories propagate back to the equilibrium configurations after hopping to the ground state, and as a result, the QY is reduced.

3.4. PetrinTzCl. Tetrazines, as ideal chromophores, are possible candidates for many applications such as protein folding, antibacterial, sensors, and high energy density materials. Meanwhile, the structure of PetrinTzCl is rather complicated, which makes it a good test system for us to study the effect of open-shell implementation on NAMD in large systems. The absorption spectra obtained from closed- and open-shell methods are the same, as shown in Figure S2, which is consistent with NM and ATTO systems. The open-shell required the calculation of 62 excited states, whereas the closed-shell required only 25 states. After photoexcitation of the tetrazine moiety, the electronic energy can remain in the tetrazine or undergo energy transfer to the Petrin portion. Previous results show that only 1 out of 300 trajectories undergoes a tetrazine ring opening phenomenon.[3] Because the electronic energy rarely results in photochemistry of the tetrazine ring, we only examine the electronic energy dissipation in the Petrin ring. After electronic energy transfer

https://dx.doi.org/10.1021/acs.jctc.9b00928
J. Chem. Theory Comput. 2020, 16, 2053−2064

to Petrin, Petrin would have stronger vibrational excitations which lead to N−O bond breaking. We used a histogram of the maximum N−O bond length to detect the N−O bond breaking events. As shown in Figure 5, the majority of N−O

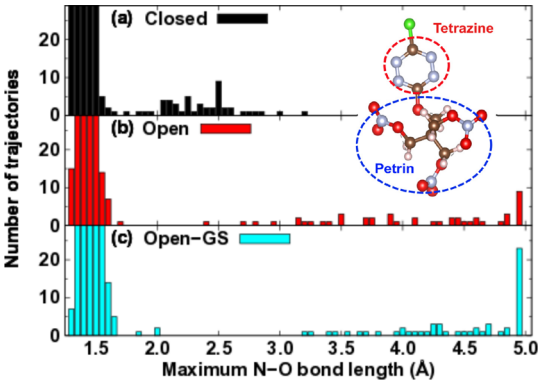

Figure 5. Histogram of the maximum N−O bond length from each NEXMD trajectory calculated from (a) closed-shell, (b) open-shell, and (c) Open-GS methods, respectively.

bond lengths resides within 1.4 to 1.6 Å. Figure 5 indicates that the open-shell method ends up with a larger probability for longer N−O bond distances. The comparison between Figure 5(b) and (c) shows that the number of trajectories with the maximum N−O distance of 2.4−3.4 Å is reduced for the Open-GS method. These trajectories either propagate forward (to longer N−O bond distances) or backward (to equilibrium geometries and shorter N−O bond distances) along the reaction coordinate. A careful examination of the 500 trajectories shows that 41, 47, and 60 trajectories in closed-shell, open-shell, and Open-GS exhibit N−O bond breaking, respectively. Open-shell exhibits slightly higher QY than closed-shell, which is consistent with the fact that UHF and UCIS establish lower reaction barriers on the ground and excited PESs. The QY for the Open-GS method is slightly increased compared to that of open-shell, which indicates that some of the trajectories with maximum N−O bond lengths in the range 2.4−3.4 Å shown in Figure 5(b) propagate forward to dissociation after hopping to the ground state in the Open-GS method.

The evolution of the excess electronic energy (compared to the ground-state S_0) and the kinetic energies from the tetrazine ring and the Petrin group for the averaged N−O bond breaking trajectories are shown in Figure 6. Both closed-shell and open-shell results show energy dissipation to vibrational motion in the Petrin group. The kinetic energy of the Petrin group exhibits a dramatic increase of about 1.2 eV, corresponding to the decrease in excess potential energy. Meanwhile, the kinetic energy of the tetrazine ring has a smaller change. In closed-shell, the electronic relaxation to S_1 is complete within 100 fs, while in open-shell, the electronic relaxation takes a longer time. The slower energy relaxation dynamics in open-shell is consistent with that of NM and ATTO due to the additional relaxation pathways caused by impure excited states (mixed excitation). As a result, the NO_2 dissociations in open-shell also occur on a longer time scale as shown by Figure S3.

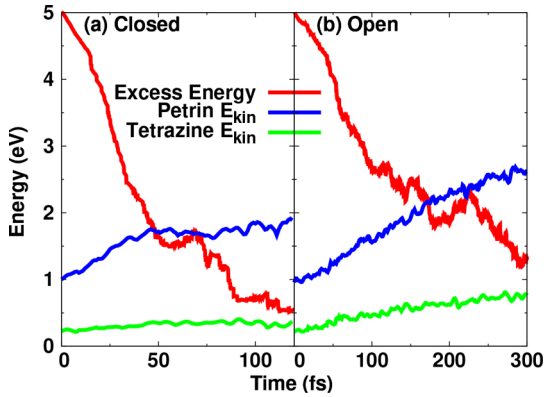

Figure 6. Evolution of the average excess electronic energy and vibrational kinetic energy contributions from a tetrazine ring and Petrin fragment for the ensemble of trajectories exhibiting NO_2 dissociation for (a) closed- and (b) open-shell simulations.

4. SUMMARY

In this work, we present NAMD methodology for unrestricted TD-SCF representation of electronically excited states, which is suitable for modeling photochemical processes in molecular materials involving bond breaking. This approach was implemented in the NEXMD[18] code, and its application to selected molecular systems undergoing photochemical reactions was demonstrated. Closed-shell descriptions assume the degeneracy of spatial orbitals of different spins; therefore, excited-state dynamics simulations based on this level of theory only follow the first bond dissociation step. Open-shell, on the other hand, can describe unpaired electrons to identify intermediate states correctly, which is demonstrated in our results. The open-shell implementation gives the same electronic structures as the closed-shell at stable equilibrium bond length regions but lower PESs at bond dissociation limits and beyond. Consequently, the simulation results show that the decay of initial excited states near equilibrium obtained from the open- and closed-shell methods is almost the same, but the overall nonadiabatic relaxation may be different because the open-shell method produces impure excited states with mixed excitations when the molecule undergoes a photochemical reaction. At the beginning of the dynamics, the pure triplet states do not contribute to the dynamics since there are no transitions between the singlet and triplet states occurring on ultrafast time scales. However, once they become impure, they can participate in the dynamics, and that slows the dynamics of open-shell simulations compared to closed-shell counterparts. Moreover, since the open-shell predicts lower PESs in all bond length regions compared to the spin-restricted closed-shell method, the reaction barrier is reduced, and consequently, the QY calculated from the open-shell simulations is usually higher than that of the closed-shell case, as confirmed by the three test cases. The direct comparisons with a closed-shell analog shown in this work demonstrate that open-shell NEXMD is more suitable for describing photochemical reactions. Even though there may be unphysical transitions between the impure states beyond the CF point, the dynamics has entered the dissociation regime. Thus, the transitions between impure states due to the spin contamination have a limited effect on the QY. Moreover, the Open-GS method can switch the dynamics to the ground-state PES once the system has reached the lowest states and beyond the CF point, which further suppresses the effect of spin

https://dx.doi.org/10.1021/acs.jctc.9b00928
J. Chem. Theory Comput. 2020, 16, 2053−2064

contamination on the chemical reactions. Nevertheless, the dynamics beyond the CF point should be checked with care to avoid significant unphysical results. In particular, description of products of chemical reactions in terms of specific spin species and radicals may be problematic due to spin contaminations, lack of spin−orbit coupling, and single-reference nature of UCIS approximation.

However, the open-shell method is more computationally expensive than the closed-shell. The reason is 2-fold. First, the spin unrestricted open-shell method does not restrict the spins in an electron pair in the same spatial orbital. Consequently, the basis set and the Liouville space in the ground- and excited-state calculations are doubled, which in turn increases the computation cost in the calculation of electronic structures. Second, the open-shell method introduces many triplet-like states which are optically inactive (dark) states. Consequently, given the same excitation energy, more states should be included in the open-shell calculation. Thus, the computational cost in the excited-state calculations is increased further. For the three example molecules studied in this work, the open-shell method is roughly 5 times more expensive than the closed-sell calculations. Since the exact number of triplet-like states in any given energy range is system dependent, there is no certain rule to determine the exact comparison.

Overall, the presented open-shell NAMD approach for excited states provides computationally efficient implementation able to treat large molecular systems with tens of excited states. However, it is a subject of considerable limitations such as spin contamination and the inability to treat crossings between excited and ground states in the TD-SCF method. Moreover, spin−orbit coupling (SOC) is not included in this work. In fact, the nonadiabatic mixed quantum-classical methods were initially developed to deal with the internal conversion which is known to be a fast nonadiabatic process. The inclusion of SOC can induce transitions between states of different multiplicities on short time scales and produce different photochemical reaction pathways (intersystem crossing).[74−77] Overcoming these limitations would constitute further improvements and practicality of the nonadiabatic mixed quantum-classical methods in future studies.

■ ASSOCIATED CONTENT

Supporting Information

The Supporting Information is available free of charge at https://pubs.acs.org/doi/10.1021/acs.jctc.9b00928.

Figures S1−S3: relative error of analytical gradient; absorption spectrum of PentrinTzCl; and time evolution of N−O bond length of trajectories that undergo N−O bond breaking (PDF)

■ AUTHOR INFORMATION

Corresponding Authors

Yu Zhang − *Physics and Chemistry of Materials, Theoretical Division, Los Alamos National Laboratory, Los Alamos, New Mexico 87545, United States;* orcid.org/0000-0001-8938-1927; Email: zhy@lanl.gov

Tammie Nelson − *Physics and Chemistry of Materials, Theoretical Division, Los Alamos National Laboratory, Los Alamos, New Mexico 87545, United States;* orcid.org/0000-0002-3173-5291; Email: tammien@lanl.gov

Authors

Linqiu Li − *Department of Chemistry, University of Southern California, Los Angeles, California 90089, United States;* orcid.org/0000-0001-9564-0577

Sergei Tretiak − *Physics and Chemistry of Materials, Theoretical Division and Center for Integrated Nanotechnologies, Los Alamos National Laboratory, Los Alamos, New Mexico 87545, United States;* orcid.org/0000-0001-5547-3647

Complete contact information is available at: https://pubs.acs.org/10.1021/acs.jctc.9b00928

Notes

The authors declare no competing financial interest.

■ ACKNOWLEDGMENTS

The work at Los Alamos National Laboratory (LANL) was supported by the LANL Directed Research and Development Funds (LDRD) and performed in part at the Center for Integrated Nanotechnologies (CINT), a U.S. Department of Energy, Office of Science user facility at LANL. This research used resources provided by the LANL Institutional Computing (IC) Program. LANL is operated by Triad National Security, LLC, for the National Nuclear Security Administration of the U.S. Department of Energy (Contract No. 89233218NCA000001).

■ REFERENCES

(1) Nelson, T.; Bjorgaard, J.; Greenfield, M.; Bolme, C.; Brown, K.; McGrane, S.; Scharff, R. J.; Tretiak, S. Ultrafast Photodissociation Dynamics of Nitromethane. *J. Phys. Chem. A* **2016**, *120*, 519−526.

(2) Lystrom, L.; Zhang, Y.; Tretiak, S.; Nelson, T. Site-Specific Photodecomposition in Conjugated Energetic Materials. *J. Phys. Chem. A* **2018**, *122*, 6055−6061.

(3) Greenfield, M. T.; McGrane, S. D.; Bolme, C. A.; Bjorgaard, J. A.; Nelson, T. R.; Tretiak, S.; Scharff, R. J. Photoactive High Explosives: Linear and Nonlinear Photochemistry of Petrin Tetrazine Chloride. *J. Phys. Chem. A* **2015**, *119*, 4846−4855.

(4) Schultz, T.; Quenneville, J.; Levine, B.; Toniolo, A.; Martínez, T. J.; Lochbrunner, S.; Schmitt, M.; Shaffer, J. P.; Zgierski, M. Z.; Stolow, A. Mechanism and Dynamics of Azobenzene Photoisomerization. *J. Am. Chem. Soc.* **2003**, *125*, 8098−8099.

(5) Levine, B. G.; MartÃnez, T. J. Isomerization Through Conical Intersections. *Annu. Rev. Phys. Chem.* **2007**, *58*, 613−634.

(6) Vincent, J. C.; Muuronen, M.; Pearce, K. C.; Mohanam, L. N.; Tapavicza, E.; Furche, F. That Little Extra Kick: Nonadiabatic Effects in Acetaldehyde Photodissociation. *J. Phys. Chem. Lett.* **2016**, *7*, 4185−4190.

(7) Fernandez-Alberti, S.; Kleiman, V. D.; Tretiak, S.; Roitberg, A. E. Unidirectional Energy Transfer in Conjugated Molecules: The Crucial Role of High-Frequency $C \equiv C$ Bonds. *J. Phys. Chem. Lett.* **2010**, *1*, 2699−2704.

(8) Li, L.; Long, R.; Prezhdo, O. V. Charge Separation and Recombination in Two-Dimensional MoS2/WS2: Time-Domain ab Initio Modeling. *Chem. Mater.* **2017**, *29*, 2466−2473.

(9) Collini, E.; Scholes, G. D. Coherent Intrachain Energy Migration in a Conjugated Polymer at Room Temperature. *Science* **2009**, *323*, 369−373.

(10) Brédas, J.-L.; Beljonne, D.; Coropceanu, V.; Cornil, J. Charge-Transfer and Energy-Transfer Processes in π−Conjugated Oligomers and Polymers: A Molecular Picture. *Chem. Rev.* **2004**, *104*, 4971−5004.

(11) Brédas, J.-L.; Silbey, R. Excitons Surf Along Conjugated Polymer Chains. *Science* **2009**, *323*, 348−349.

(12) Tretiak, S.; Saxena, A.; Martin, R. L.; Bishop, A. R. Conformational Dynamics of Photoexcited Conjugated Molecules. *Phys. Rev. Lett.* **2002**, *89*, 097402.

(13) Crespo-Otero, R.; Barbatti, M. Recent Advances and Perspectives on Nonadiabatic Mixed Quantum-Classical Dynamics. *Chem. Rev.* **2018**, *118*, 7026−7068.
(14) Curchod, B. F. E.; Martínez, T. J. Ab Initio Nonadiabatic Quantum Molecular Dynamics. *Chem. Rev.* **2018**, *118*, 3305−3336.
(15) Tully, J. C. Perspective: Nonadiabatic Dynamics Theory. *J. Chem. Phys.* **2012**, *137*, 22A301.
(16) Sifain, A. E.; Bjorgaard, J. A.; Nelson, T. R.; Nebgen, B. T.; White, A. J.; Gifford, B. J.; Gao, D. W.; Prezhdo, O. V.; Fernandez-Alberti, S.; Roitberg, A. E.; Tretiak, S. Photoexcited Nonadiabatic Dynamics of Solvated Push-Pull π−Conjugated Oligomers with the NEXMD Software. *J. Chem. Theory Comput.* **2018**, *14*, 3955−3966.
(17) Nelson, T.; Fernandez-Alberti, S.; Chernyak, V.; Roitberg, A. E.; Tretiak, S. Nonadiabatic Excited-State Molecular Dynamics: Numerical Tests of Convergence and Parameters. *J. Chem. Phys.* **2012**, *136*, 054108.
(18) Nelson, T.; Fernandez-Alberti, S.; Roitberg, A. E.; Tretiak, S. Nonadiabatic Excited-State Molecular Dynamics: Modeling Photophysics in Organic Conjugated Materials. *Acc. Chem. Res.* **2014**, *47*, 1155−1164.
(19) Tully, J. C. Molecular Dynamics with Electronic Transitions. *J. Chem. Phys.* **1990**, *93*, 1061−1071.
(20) Antol, I.; Eckert-Maksić, M.; Barbatti, M.; Lischka, H. Simulation of the Photodeactivation of Formamide in the $n_O - \pi^*$ and $\pi - \pi^*$states: An ab Initio On-the-Fly Surface-Hopping Dynamics Study. *J. Chem. Phys.* **2007**, *127*, 234303.
(21) Prezhdo, O. V. Photoinduced Dynamics in Semiconductor Quantum Dots: Insights from Time-Domain ab Initio Studies. *Acc. Chem. Res.* **2009**, *42*, 2005−2016.
(22) Subotnik, J. E.; Jain, A.; Landry, B.; Petit, A.; Ouyang, W.; Bellonzi, N. Understanding the Surface Hopping View of Electronic Transitions and Decoherence. *Annu. Rev. Phys. Chem.* **2016**, *67*, 387−417.
(23) Barbatti, M. Nonadiabatic Dynamics with Trajectory Surface Hopping Method. *WIREs: Comp. Mol. Sci.* **2011**, *1*, 620−633.
(24) Tavernelli, I.; Curchod, B. F. E.; Laktionov, A.; Rothlisberger, U. Nonadiabatic Coupling Vectors for Excited States within Time-Dependent Density Functional Theory in the Tamm-Dancoff Approximation and beyond. *J. Chem. Phys.* **2010**, *133*, 194104.
(25) Furche, F. On the Density Matrix based Approach to Time-dependent Density Functional Response Theory. *J. Chem. Phys.* **2001**, *114*, 5982−5992.
(26) Furche, F.; Ahlrichs, R. Adiabatic Time-Dependent Density Functional Methods for Excited State Properties. *J. Chem. Phys.* **2002**, *117*, 7433−7447.
(27) Tretiak, S.; Chernyak, V.; Mukamel, S. Recursive Density-Matrix-Spectral-Moment Algorithm for Molecular Nonlinear Polarizabilities. *J. Chem. Phys.* **1996**, *105*, 8914−8928.
(28) Smith, B. R.; Bearpark, M. J.; Robb, M. A.; Bernardi, F.; Olivucci, M. Classical Wavepacket Dynamics through a Conical Intersection-Application to the S1/S0 Photochemistry of Benzene. *Chem. Phys. Lett.* **1995**, *242*, 27−32.
(29) Pratihar, S.; Ma, X.; Homayoon, Z.; Barnes, G. L.; Hase, W. L. Direct Chemical Dynamics Simulations. *J. Am. Chem. Soc.* **2017**, *139*, 3570−3590.
(30) Akimov, A. V.; Prezhdo, O. V. The PYXAID Program for Non-Adiabatic Molecular Dynamics in Condensed Matter Systems. *J. Chem. Theory Comput.* **2013**, *9*, 4959−4972.
(31) Prezhdo, O. V.; Duncan, W. R.; Prezhdo, V. V. Dynamics of the Photoexcited Electron at the Chromophore£Semiconductor Interface. *Acc. Chem. Res.* **2008**, *41*, 339−348.
(32) Akimov, A. V.; Neukirch, A. J.; Prezhdo, O. V. Theoretical Insights into Photoinduced Charge Transfer and Catalysis at Oxide Interfaces. *Chem. Rev.* **2013**, *113*, 4496−4565.
(33) Schmidt, M. W.; Gordon, M. S. The Construction and Interpretation of MCSCF Wavefunctions. *Annu. Rev. Phys. Chem.* **1998**, *49*, 233−266.
(34) Gagliardi, L.; Truhlar, D. G.; Li Manni, G.; Carlson, R. K.; Hoyer, C. E.; Bao, J. L. Multiconfiguration Pair-Density Functional Theory: A New Way To Treat Strongly Correlated Systems. *Acc. Chem. Res.* **2017**, *50*, 66−73.
(35) Dewar, M. J. S.; Zoebisch, E. G.; Healy, E. F.; Stewart, J. J. P. Development and Use of Quantum Mechanical Molecular Models. 76. AM1: a New General Purpose Quantum Mechanical Molecular Model. *J. Am. Chem. Soc.* **1985**, *107*, 3902−3909.
(36) Tretiak, S.; Isborn, C. M.; Niklasson, A. M. N.; Challacombe, M. Representation Independent Algorithms for Molecular Response Calculations in Time-Dependent Self-Consistent Field Theories. *J. Chem. Phys.* **2009**, *130*, 054111.
(37) Chernyak, V.; Schulz, M. F.; Mukamel, S.; Tretiak, S.; Tsiper, E. V. Krylov-Space Algorithms for Time-Dependent Hartree-Fock and Density Functional Computations. *J. Chem. Phys.* **2000**, *113*, 36−43.
(38) Hirata, S.; Head-Gordon, M.; Bartlett, R. J. Configuration Interaction Singles, Time-Dependent Hartree-Fock, and Time-Dependent Density Functional Theory for the Electronic Excited States of Extended Systems. *J. Chem. Phys.* **1999**, *111*, 10774−10786.
(39) Tapavicza, E.; Bellchambers, G. D.; Vincent, J. C.; Furche, F. Ab Initio Non-Adiabatic Molecular Dynamics. *Phys. Chem. Chem. Phys.* **2013**, *15*, 18336−18348.
(40) Han, Y.; Rasulev, B.; Kilin, D. S. Photofragmentation of Tetranitromethane: Spin-Unrestricted Time-Dependent Excited-State Molecular Dynamics. *J. Phys. Chem. Lett.* **2017**, *8*, 3185−3192.
(41) Han, Y.; Rasulev, B.; Kilin, D. S. Photofragmentation of Tetranitromethane: Spin-Unrestricted Time-Dependent Excited-State Molecular Dynamics. *J. Phys. Chem. Lett.* **2017**, *8*, 3185−3192.
(42) Bjorgaard, J. A.; Kuzmenko, V.; Velizhanin, K. A.; Tretiak, S. Solvent Effects in Time-Dependent Self-Consistent Field Methods. I. Optical Response Calculations. *J. Chem. Phys.* **2015**, *142*, 044103.
(43) Tretiak, S.; Mukamel, S. Density Matrix Analysis and Simulation of Electronic Excitations in Conjugated and Aggregated Molecules. *Chem. Rev.* **2002**, *102*, 3171−3212.
(44) Tretiak, S.; Chernyak, V. Resonant Nonlinear Polarizabilities in the Time-Dependent Density Functional Theory. *J. Chem. Phys.* **2003**, *119*, 8809−8823.
(45) Nelson, T.; Fernandez-Alberti, S.; Chernyak, V.; Roitberg, A. E.; Tretiak, S. Nonadiabatic Excited-State Molecular Dynamics Modeling of Photoinduced Dynamics in Conjugated Molecules. *J. Phys. Chem. B* **2011**, *115*, 5402−5414.
(46) Stratmann, R. E.; Scuseria, G. E.; Frisch, M. J. An Efficient Implementation of Time-Dependent Density-Functional Theory for the Calculation of Excitation Energies of Large Molecules. *J. Chem. Phys.* **1998**, *109*, 8218−8224.
(47) Maurice, D.; Head-Gordon, M. Configuration Interaction with Single Substitutions for Excited States of Open-Shell Molecules. *Int. J. Quantum Chem.* **1995**, *56*, 361−370.
(48) Dunning, T. H.; McKoy, V. Nonempirical Calculations on Excited States: The Ethylene Molecule. *J. Chem. Phys.* **1967**, *47*, 1735−1747.
(49) Dunning, T. H.; McKoy, V. Nonempirical Calculations on Excited States: The Formaldehyde Molecule. *J. Chem. Phys.* **1968**, *48*, 5263−5270.
(50) Szabo, A.; Ostlund, N. S. *Modern Quantum Chemistry: Introduction to Advanced Electronic Structure Theory*, 1st ed.; Dover Publications, Inc.: Mineola, 1996.
(51) Feynman, R. P. Forces in Molecules. *Phys. Rev.* **1939**, *56*, 340−343.
(52) van der Vorst, H. Bi-CGSTAB: A Fast and Smoothly Converging Variant of Bi-CG for the Solution of Nonsymmetric Linear Systems. *SIAM J. Sci. Stat. Comput.* **1992**, *13*, 631−644.
(53) Chernyak, V.; Mukamel, S. Density-Matrix Representation of Nonadiabatic Couplings in Time-Dependent Density Functional (TDDFT) Theories. *J. Chem. Phys.* **2000**, *112*, 3572−3579.
(54) Tommasini, M.; Chernyak, V.; Mukamel, S. Electronic density-matrix algorithm for nonadiabatic couplings in molecular dynamics simulations. *Int. J. Quantum Chem.* **2001**, *85*, 225−238.
(55) Freixas, V. M.; Fernandez-Alberti, S.; Makhov, D. V.; Tretiak, S.; Shalashilin, D. An ab Initio Multiple Cloning Approach for the

https://dx.doi.org/10.1021/acs.jctc.9b00928
J. Chem. Theory Comput. 2020, 16, 2053−2064

Simulation of Photoinduced Dynamics in conjugated molecules. *Phys. Chem. Chem. Phys.* **2018**, *20*, 17762−17772.
(56) Makhov, D. V.; Glover, W. J.; Martinez, T. J.; Shalashilin, D. V. Ab Initio Multiple Cloning Algorithm for Quantum Nonadiabatic Molecular Dynamics. *J. Chem. Phys.* **2014**, *141*, 054110.
(57) Fernandez-Alberti, S.; Makhov, D. V.; Tretiak, S.; Shalashilin, D. V. Non-Adiabatic Excited State Molecular Dynamics of Phenylene Ethynylene Dendrimer using a Multiconfigurational Ehrenfest Approach. *Phys. Chem. Chem. Phys.* **2016**, *18*, 10028−10040.
(58) Nelson, T.; Fernandez-Alberti, S.; Roitberg, A. E.; Tretiak, S. Nonadiabatic Excited-State Molecular Dynamics: Treatment of Electronic Decoherence. *J. Chem. Phys.* **2013**, *138*, 224111.
(59) Fernandez-Alberti, S.; Roitberg, A. E.; Nelson, T.; Tretiak, S. Identification of Unavoided Crossings in Nonadiabatic Photoexcited Dynamics Involving Multiple Electronic States in Polyatomic Conjugated Molecules. *J. Chem. Phys.* **2012**, *137*, 014512.
(60) Levine, B. G.; Ko, C.; Quenneville, J.; MartÍnez, T. J. Conical Intersections and Double Excitations in Time-Dependent Density Functional Theory. *Mol. Phys.* **2006**, *104*, 1039−1051.
(61) Kabadi, V. N.; Rice, B. M. Molecular Dynamics Simulations of Normal Mode Vibrational Energy Transfer in Liquid Nitromethane. *J. Phys. Chem. A* **2004**, *108*, 532−540.
(62) Dawes, R.; Siavosh-Haghighi, A.; Sewell, T. D.; Thompson, D. L. Shock-Induced Melting of (100)-Oriented Nitromethane: Energy Partitioning and Vibrational Mode Heating. *J. Chem. Phys.* **2009**, *131*, 224513.
(63) Gruzdkov, Y. A.; Gupta, Y. M. Emission and Fluorescence Spectroscopy To Examine Shock-Induced Decomposition in Nitromethane. *J. Phys. Chem. A* **1998**, *102*, 8325−8332.
(64) Blais, N. C.; Engelke, R.; Sheffield, S. A. Mass Spectroscopic Study of the Chemical Reaction Zone in Detonating Liquid Nitromethane. *J. Phys. Chem. A* **1997**, *101*, 8285−8295.
(65) Ravensbergen, J.; Abdi, F. F.; van Santen, J. H.; Frese, R. N.; Dam, B.; van de Krol, R.; Kennis, J. T. M. Unraveling the Carrier Dynamics of BiVO4: A Femtosecond to Microsecond Transient Absorption Study. *J. Phys. Chem. C* **2014**, *118*, 27793−27800.
(66) Guo, Y. Q.; Bhattacharya, A.; Bernstein, E. R. Photodissociation Dynamics of Nitromethane at 226 and 271 nm at Both Nanosecond and Femtosecond Time Scales. *J. Phys. Chem. A* **2009**, *113*, 85−96.
(67) Myneni, H.; Casida, M. E. On the calculation of $\Delta < S^2 >$ for electronic excitations in time-dependent density-functional theory. *Comput. Phys. Commun.* **2017**, *213*, 72−91.
(68) Foresman, J. B.; Schlegel, H. B. In *Recent Experimental and Computational Advances in Molecular Spectroscopy*; Fausto, R., Ed.; Springer Netherlands: Dordrecht, 1993; pp 11−26, DOI: 10.1007/978-94-011-1974-0_2.
(69) Hait, D.; Rettig, A.; Head-Gordon, M. Beyond the Coulson-Fischer Point: Characterizing Single Excitation CI and TDDFT for Excited States in Single Bond Dissociations. *Phys. Chem. Chem. Phys.* **2019**, *21*, 21761−21775.
(70) *BAGEL: Brilliantly Advanced General Electronic-structure Library*. http://www.nubakery.org (accessed 2020-03-09).
(71) Shiozaki, T. BAGEL: Brilliantly Advanced General Electronic-structure Library. *Wiley Interdiscip. Rev.: Comput. Mol. Sci.* **2018**, *8*, No. e1331.
(72) Shiozaki, T.; Győrffy, W.; Celani, P.; Werner, H.-J. Communication: Extended Multi-State Complete Active Space Second-Order Perturbation Theory: Energy and Nuclear Gradients. *J. Chem. Phys.* **2011**, *135*, 081106.
(73) Bjorgaard, J. A.; Sifain, A. E.; Nelson, T.; Myers, T. W.; Veauthier, J. M.; Chavez, D. E.; Scharff, R. J.; Tretiak, S. Two-Photon Absorption in Conjugated Energetic Molecules. *J. Phys. Chem. A* **2016**, *120*, 4455−4464.
(74) Richter, M.; Marquetand, P.; González-Vázquez, J.; Sola, I.; González, L. SHARC: ab Initio Molecular Dynamics with Surface Hopping in the Adiabatic Representation Including Arbitrary Couplings. *J. Chem. Theory Comput.* **2011**, *7*, 1253−1258.
(75) Mai, S.; Marquetand, P.; González, L. A General Method to Describe Intersystem Crossing Dynamics in Trajectory Surface Hopping. *Int. J. Quantum Chem.* **2015**, *115*, 1215−1231.
(76) Franco de Carvalho, F.; Tavernelli, I. Nonadiabatic Dynamics with Intersystem Crossings: A Time-Dependent Density Functional Theory Implementation. *J. Chem. Phys.* **2015**, *143*, 224105.
(77) Cui, G.; Thiel, W. Generalized Trajectory Surface-Hopping Method for Internal Conversion and Intersystem Crossing. *J. Chem. Phys.* **2014**, *141*, 124101.

https://dx.doi.org/10.1021/acs.jctc.9b00928
J. Chem. Theory Comput. 2020, 16, 2053−2064